

# An Exact Continuous Theory for Spin Systems on Graphons

Amy Searle<sup>1</sup> and Joseph Tindall<sup>2</sup>

<sup>1</sup>*Department of Physics, University of Oxford, OX1 3PU*

<sup>2</sup>*Center for Computational Quantum Physics, Flatiron Institute, 162 5th Avenue, New York, NY 10010 \**

(Dated: March 2, 2023)

We formulate a general, continuous description of quantum spin systems in thermal equilibrium when the average co-ordination number grows extensively in the system size. Specifically, for sequences of dense graphs whose properties converge in the thermodynamic limit we derive an elegant set of three coupled non-linear Fredholm integral equations which govern the properties of the system. In these equations the graphon, a continuous mathematical object recently developed to describe such dense graph sequences, forms the kernel and their solution yields exact expressions for the macroscopic observables in the system in the thermodynamic limit. We analyse these equations for systems such as the classical and transverse field Ising models, demonstrating how the integral equations easily recover known results as well as providing analytical solutions for a range of more complex cases. We also perform finite-size numerical calculations with Monte-Carlo and Tensor Network methods and show their convergence towards our analytical results.

*Introduction* – The physical properties manifested by interacting systems are strongly controlled by the connectivity of their components. For instance, network topology plays a decisive role in the rate of disease spreading in infectious disease models [1] whilst systematic studies have been undertaken into the effect of connectivity on the ability of oscillators to synchronise [2–5].

In Condensed Matter Physics, the same ideas hold true. The exotic properties exhibited by many-body Hamiltonians—such as unconventional superconductivity [6] and boundary-confined conductivity [7]—are known to depend delicately upon the details of the network topology. While such results have had significant impact on the field, a more general formalism and characterisation of how network topology influences strongly correlated systems is unknown. The absence of such a formalism is attributable to the difficulty of solving the many-body problem—making general, mathematical studies of different geometries exceptionally difficult.

In the regime where disorder is absent and the average co-ordination number becomes large, however, many-body systems fall into the mean-field universality class and become amenable to simpler, mathematical and computational approaches [8–12]. Despite usually being applied to translationally-invariant systems, the mean field approach is known to be valid for the infinite multitude of networks, whether homogeneous or heterogeneous[13], where the average co-ordination number is proportional to the system size [14]. Moreover, within the field of graph theory, such structures are well-characterised with their thermodynamic limit being elegantly described by the graphon [15, 16], a continuous mathematical object introduced which describes the limit of the adjacency matrix of a dense (i.e. one where the average co-ordination number is proportional to the graph size) graph as the number of vertices tends to infinity. Since its inception,

this mathematical object has been utilised in the study of classical synchronisation, the dynamics of power networks and game theory [17–19], to name a few examples.

Motivated by these ideas we, for the first time [20], utilise the graphon in the study of interacting spin systems. Specifically, we take a very general spin Hamiltonian defined over an arbitrary graph and, for any given sequence of dense graphs whose limit is known to converge to a given graphon, we derive a coupled set of integral equations which exactly describe the equilibrium physics of the system in the thermodynamic limit. The graphon forms the kernel in these integral equations and the Physics of the system can be directly studied as a function of this object—with a given graphon always defining a sequence of finite graphs whose thermodynamic limit is that graphon. Taking several example spin models such as the classical and Transverse Field Ising model we demonstrate the utility of these integral equations: i) verifying previous results on all-to-all spin systems, ii) proving the existence of a finite-temperature phase transition in the classical Ising model for any graphon and iii) deriving analytical solutions for the equilibrium observables of non-trivial, heterogeneous networks. We reinforce our analytical solutions with large-scale, finite-size Monte Carlo and Tensor Network simulations. We emphasize that whilst the spin systems we treat in this work are commonly studied in Condensed Matter Physics due to their relevance as models of real-world magnetism, they also find application in many other branches of science, including the political, social and biological sciences [21–23].

*Hamiltonian* – Our starting point is that of  $L$  qubits placed on the  $L$  vertices of a weighted graph  $G_L$ . The graph is completely specified by an  $L \times L$  symmetric adjacency matrix  $A_{GL}$  with elements  $A_{v,v'}$  which dictate the weighted connections between vertices (qubits)  $v, v'$ ,

---

\* [jtindall@flatironinstitute.org](mailto:jtindall@flatironinstitute.org)

with  $v, v' = 1 \dots L$ . The Hamiltonian reads

$$H(G_L) = \frac{1}{L} \sum_{\substack{v, v'=1 \\ v > v'}}^L A_{v, v'} \left( \sum_{\alpha=x, y, z} J^\alpha \hat{\sigma}_v^\alpha \hat{\sigma}_{v'}^\alpha \right) + \sum_{\substack{v \in V \\ \alpha=x, y, z}} h^\alpha \hat{\sigma}_v^\alpha. \quad (1)$$

where  $J^\alpha$  and  $h^\alpha$  are real valued and  $\hat{\sigma}_v^\alpha$  is the Pauli spin operator acting on the spin on vertex  $v$ . Our focus here is exclusively on graphs where  $0 \leq A_{v, v'} \leq 1$  and  $\sum_{v, v'} A_{v, v'} \propto L^2$ . We refer to these as ‘dense’ graphs because the average co-ordination number diverges with system size. The factor of  $\frac{1}{L}$  in  $H(G_L)$  is necessary in this case to ensure the energy density of any normalised state remains finite and non-trivial.

*Theory* – In this work, by utilising tools from graph theory and applying mean-field theory, we formulate an explicit, exact, continuous description of this system in thermal equilibrium in the thermodynamic limit. Such a description is powerful, in the sense it can be applied to an enormous range of graphs  $G_L$  and in certain cases, be used to derive analytical expressions for observables in the system.

In order to introduce our continuum description, we take the vertices (qubits) of the graph  $G_L$ ,  $v = 1 \dots L$  and transform them as  $x = v/L \in [0, 1]$ . We then define  $W_{G_L}(x, y) : [0, 1]^2 \rightarrow [0, 1]$  which is a real symmetric stepped function over the unit square such that for a given  $(x, y) \in I_v \times I_{v'}$ , where  $I_v = [(v-1)/L, v/L]$  then  $W_{G_L}(x, y) = A_{v, v'}$ .

Equipped with a well-defined metric for the similarity of two graphs, it can be shown that for certain sequences of graphs  $(G_L)_{L \in \mathbb{N}}$  the limit  $\lim_{L \rightarrow \infty} W_{G_L}(x, y)$  converges to a well-defined symmetric function  $W(x, y)$  known as the ‘graphon’ [15, 16]. Specifically, given two dense graphs  $G_A$  and  $G_B$  defined over the same vertex set  $V = \{1 \dots L\}$ , there are two choices of metric for this similarity. The first is the ‘cut distance’ which averages, over all pairs of subsets of  $V$ , the difference in the fraction of edges between the two subgraphs induced on  $G_A$  and  $G_B$ . The second is the ‘homomorphism density’ which averages, over all possible subgraphs  $F$ , the difference between the number of instances of  $F$  on  $G_A$  and  $G_B$ . It is known that if a sequence of dense graphs converges under one of these metrics then they also converge under the other. Further mathematical details and theorems on these notions of convergence are provided in the Appendix.

Importantly, given a graphon  $W(x, y)$  one can also construct a corresponding ‘exchangeable random graph model’  $G_L^R$ , which is a finite random realisation of  $W(x, y)$  over  $L$  vertices indexed as  $v = 1 \dots L$ . This is achieved by defining the quantity

$$P_{v, v'} = L^2 \int_{I_v \times I_{v'}} W(x, y) dx dy, \quad I_v = [(v-1)/L, v/L], \quad (2)$$

and building the adjacency matrix of  $G_L^R$  by setting  $A_{v, v'} = 1$  with probability  $P_{v, v'}$  and  $A_{v, v'} = 0$  otherwise.

A given sequence of such random realisations  $(G_L^R)_{L \in \mathbb{N}}$  is guaranteed to converge to the graphon  $W(x, y)$  in the limit  $L \rightarrow \infty$ .

The central result of this paper is that for a given graph  $G_L^R$  which is a finite realisation of some graphon  $W(x, y)$ , the equilibrium physics at inverse temperature  $\beta$  of  $H(G_L^R)$  in the thermodynamic limit is completely determined by the solution of a set of integral equations whose kernel is given by the graphon  $W(x, y)$ .

In order to reach these equations we first present the following theorem which we prove in the appendix

**Theorem 1** *Let  $f(A) = -\frac{1}{L\beta} \ln(\text{Tr}(\exp(-\beta A)))$  be the free energy density of a  $d^L \times d^L$  matrix, with  $\beta \in \mathbb{R}_{\geq 0}$ . Let  $G_L^R$  be the random-exchange realisation on  $L$  vertices of a graphon  $W(x, y)$ . Let  $G_L^D$  be a weighted graph on  $L$  vertices whose adjacency matrix  $A^D$  is specified by the elements  $A_{v, v'}^D = P_{v, v'}$ , with  $P_{v, v'}$  defined from  $W(x, y)$  as in Eq. (2). Then for an arbitrary set of real, finite values for the parameters  $\{J^x, J^y, J^z, h^x, h^y, h^z\}$  the following is true*

$$|f(H(G_L^R)) - f(H(G_L^D))| = \mathcal{O}(L^{-1/2}), \quad (3)$$

which vanishes in the limit  $L \rightarrow \infty$ .

This theorem allows us to focus entirely on the simpler, non-random Hamiltonian  $H(G_L^D)$  when determining the equilibrium properties (at least those that can be derived from the free energy density) of  $H(G_L^R)$  as  $L \rightarrow \infty$ .

Due to the dense, positive nature of the interactions a mean-field treatment of  $H(G_L^D)$  is valid in the sense that it can exactly capture the expectation value of observables at any inverse temperature  $\beta$  [14] as  $L \rightarrow \infty$ . We derive these mean-field equations explicitly in the appendix by: performing the substitution  $\hat{\sigma}_v^\alpha = \langle \hat{\sigma}_v^\alpha \rangle + \hat{\delta}_v^\alpha$  into  $H(G_L^D)$ , ignoring terms of order  $\hat{\delta}^2$ , constructing the equilibrium state of the system, deriving self-consistent equations for the observables  $\langle \hat{\sigma}_v^\alpha \rangle$ , and then taking the continuum limit of these equations. The result is the following three non-linear Fredholm self-consistent integral equations

$$\lambda^\alpha(x) = -J^\alpha \int_0^1 \frac{W(x, y) \lambda^\alpha(y) \tanh(\beta \Lambda(y))}{\Lambda(y)} dy + h^\alpha, \quad (4)$$

with  $\alpha = x, y, z$ ,  $\Lambda(x) = \sqrt{(\lambda^x(x))^2 + (\lambda^y(x))^2 + (\lambda^z(x))^2}$  [24] and the three functions  $\lambda^\alpha(x)$  each being continuous, real-valued and defined over the domain  $[0, 1]$ . If we can solve Eq. (4) for these functions, then we have determined the equilibrium physics of  $H(G_L^R)$  in the thermodynamic limit. This is because these functions directly encode the physical properties of the equilibrium state. For instance, the total magnetisation density  $M^\alpha = \frac{1}{L} \sum_{v=1}^L \sigma_v^\alpha$  in the  $\alpha = x, y$  or  $z$  directions can be expressed as

$$M^\alpha = \lim_{L \rightarrow \infty} \frac{1}{L} \sum_{v=1}^L \sigma_v^\alpha = - \int_0^1 \frac{\lambda^\alpha(x) \tanh(\Lambda(x))}{\Lambda(x)} dx. \quad (5)$$

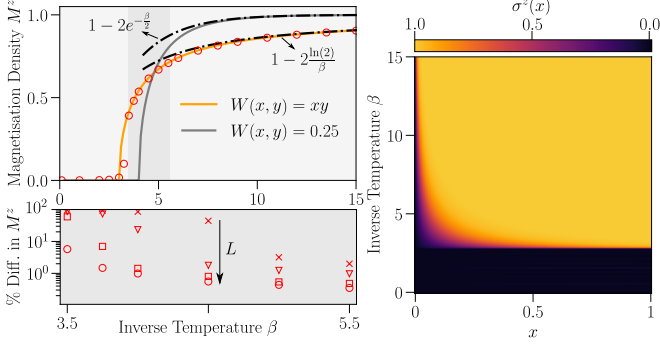


FIG. 1. Magnetisation of the classical Ising model for two different choices of graphon,  $W(x, y) = xy$  and  $W(x, y) = \frac{1}{4}$ . **a)** Total Magnetisation density in the thermodynamic limit for the two graphons. Black dashed-dotted lines give the asymptotic derived by taking the large  $\beta$  limit of the respective closed-form equations. Red circles correspond to Monte Carlo simulations of finite,  $L = 800$ , random exchange models derived from  $W(x, y) = xy$ . Bottom) Percentage difference in  $M^z$  for the exact result in the thermodynamic limit versus finite-size Monte Carlo simulations at several  $L$  (crosses are  $L = 100$ , triangles  $L = 200$ , squares  $L = 400$  and circles  $L = 800$ ). For each  $\beta$  and  $L$ , 100 random exchange models are realised and the data (both top and bottom plots) is averaged over these. Details of errors and numerical parameters are provided in the appendix. **b)** On-site magnetisation  $\sigma^z(x)$  versus  $\beta$  and  $x$  for the graphon  $W(x, y) = xy$  in the thermodynamic limit.

How can we solve these equations? In general there is no analytical solution to such equations and we will be restricted to numerical methods. Nonetheless, there are certain cases where they can be solved analytically. For example, consider the case the graphon is degenerate, i.e.  $W(x, y) = \sum_{i=1}^n f_i(x)f_i(y)$  where  $n$  is finite and  $f_i(x) : [0, 1] \rightarrow [0, 1]$ . Substitution into the above equation tells us that  $\lambda^\alpha(x) = \sum_{i=1}^n c_i^\alpha f_i(x)$  where  $c_i^\alpha$  are real-valued coefficients which depend on the field strengths  $h^\alpha$ , couplings  $J^\alpha$  and the inverse temperature  $\beta$  but do not depend on  $x$ . These coefficients  $c_i^\alpha$  are obtained as the solution of the set of  $3n$  coupled equations which result from the substitution of  $\lambda^\alpha(x) = \sum_{i=1}^n c_i^\alpha f_i(x)$  into Eq.(4). For a given set of  $J^\alpha$ ,  $h^\alpha$  and value of  $\beta$  we therefore have a closed form for  $\lambda^\alpha(x)$  and various observables in the system.

*Classical Ising Model* – We will now highlight the power of the equations we have derived by considering some specific limits of Eq. (1). As our first example model we set  $J^x = J^y = h^x = h^y = h^z = 0$  and  $J^z = -1$ , realising the classical Ising model with zero field. Utilising  $\text{sgn}(z) \tanh(\beta|z|) = \tanh(z)$ , our integral equations reduce to the single equation

$$\lambda^z(x) = \int_0^1 W(x, y) \tanh(\beta \lambda^z(y)) dy. \quad (6)$$

The  $\mathbb{Z}_2$  spin-flip symmetry of the model is encoded in the fact that if  $\lambda^z(x)$  is a solution to the equation then so is

$-\lambda^z(x)$ . Moreover, there is clearly always the trivial solution  $\lambda^z(x) = 0 \forall x$  which corresponds to the disordered paramagnetic state with 0 magnetisation. Applying Banach's fixed-point theorem [25] to Eq. (6) tells us that, with certainty, when  $\beta < \sup_{x \in [0, 1]} \int_0^1 W(x, y) dx$  this is the only solution. For larger values of  $\beta$ , however, there can thus exist a non-trivial solution which corresponds to a ferromagnetic phase. For instance, when  $\beta \rightarrow \infty$  we have  $\lambda^z(x) = \int_0^1 W(x, y) dx \neq 0 \forall x$ . Thus, following this analysis, we know that  $\lambda^z(x, \beta)$  (we introduce the  $\beta$  to denote the dependence on  $\beta$ ) cannot be smooth and continuous over  $x \in [0, 1]$  and  $\beta \in [0, \infty]$  and there must exist a finite-order transition between the ferromagnetic solution and the paramagnetic solution at some critical temperature. Our continuum description has therefore allowed us to prove the existence of a ferromagnetic-paramagnetic phase transition for the Ising model on *any* dense graph—with a corresponding analytical upper bound on this temperature. A similar argument can be applied to a number of the spin model limits of Eq. (1), not just the classical Ising model.

Now let us treat some explicit examples. We first consider  $W(x, y) = p$  whose random exchange realisations is  $G_{\text{ER}}(p)$ : the Erdős-Rényi graph over  $L$  vertices where each edge appears independently with probability  $p$ . It is straightforward to observe from Eq. (6) that in this case  $\lambda^z(x) = \lambda^z = p \tanh(\beta \lambda^z)$  and is independent of  $x$ . Substituting this into Eq. (5) leads us to the familiar self-consistent equation  $M^z = \tanh(\beta p M^z)$  for the magnetisation  $M^z$  of the Classical Ising model under the mean-field approximation. The edge probability  $p$  simply acts like a re-scaling of temperature in the all-to-all model and the randomness of the model has no effect on the macroscopic physics in the thermodynamic limit—a result which has been proven to be general for spin systems on Erdős-Rényi graphs [26, 27].

Let us now move on to the more complex, unstudied, case  $W(x, y) = xy$ . Here we have a graphon whose random exchange model dictates that each pair of spins  $v$  and  $v'$  interacts with a strength 1 with probability  $(vv'/L^2)$  and strength 0 otherwise. One can also choose to directly interpret the deterministic realisation of the graphon, where each pair of spins interacts with a strength  $(vv'/L^2)$ . Both interpretations lead to the same physics in the thermodynamic limit—this follows directly from Theorem 1. In this case we derive from Eq. (6) (see Appendix)  $\sigma^z(x) = \tanh(\beta cx)$  and  $M^z = \frac{\ln(\cosh(c))}{c}$  where  $c$  is the real-valued solution of the equation

$$\frac{1}{24c^3}(12c^2 - \pi^2 + 24\text{cln}(1 + e^{-2c}) - 12\text{PL}_2(-e^{-2c}) = \frac{1}{\beta}, \quad (7)$$

and  $\text{PL}_2$  is the PolyLogarithm function of order 2. We can do much better than Banach's fixed point theorem and get an exact analytical expression for the critical inverse temperature here, not just a lower bound. Specifically,  $\beta_c$  is the superimum of the LHS of the above equation for  $c \in [0, \infty]$ , which gives us  $\beta_c = 3$ .

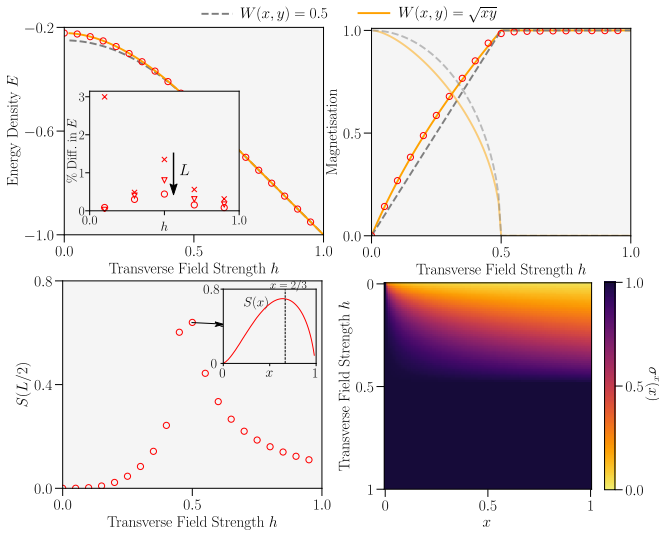


FIG. 2. **a)** Energy density of the ground state of the transverse field Ising model for two different choices of graphon,  $W(x,y) = \sqrt{xy}$  and  $W(x,y) = \frac{1}{2}$ . Lines represent analytic solutions in the thermodynamic limit whilst the markers represent numerical calculations for finite-realisations of  $W(x,y)$  over  $L = 100$  sites. Inset) Percentage difference for the ground state energy calculated on  $L = 25, 50$  and  $100$  (cross, triangle and square marker respectively) site random-exchange realisations of  $W(x,y)$  vs the exact solution in the thermodynamic limit. **b)** Total transverse (unfaded) and longitudinal (faded) Magnetisation densities of the ground state. **c)** Average Von Neumann Entanglement Entropy between two halves of the system for finite realisations of  $W(x,y) = \sqrt{xy}$  over  $L = 100$  sites. Inset) Von-Neumann Entropy vs Partition Size ( $x = A/L$ , where  $A = 1\dots L$  is the number of sites in the partition) at the critical point  $h = 0.5$  **d)** Analytical result for the on-site magnetisation  $\sigma^x(x)$  versus transverse field strength  $h$  and position  $x$  for the graphon  $W(x,y) = \sqrt{xy}$ . Finite-size numerical calculations were done by using the DMRG algorithm on random-exchange realisations of  $W(x,y)$  on  $L$  sites and averaged over 50 disorders. Further details can be found in the appendix.

In Fig. 1 we plot both the total magnetisation  $M^z$  and the local magnetisation  $\sigma^z(x)$  versus  $\beta$  based on our analytical solution. We also perform finite-size Monte-Carlo numerics for  $M^z$  for increasing system size and demonstrate convergence to our analytical solution. We compare these results to the graphon  $W(x,y) = 0.25$ . As the temperature increases both systems undergo a second-order phase transition characterised by typical mean-field exponents. For the graphon  $W(x,y) = xy$ , however, the convergence to a fully ferromagnetic state at zero temperature is much slower. This convergence can be determined analytically by expanding Eq. (7) for large  $\beta$  and substituting it into  $M^z = \frac{\ln(\cosh(c))}{c}$ , yielding  $M^z = 1 - \frac{2\ln(2)}{\beta}$ . There is thus a direct linear convergence of the magnetisation to 1 with temperature  $T = \frac{1}{\beta}$  versus the exponentially fast convergence associated with the homogeneous  $W(x,y) = \text{const.}$  case.

This slow convergence is a direct result of the ‘left boundary’ of the system. In Fig. 1b) we see that the local magnetisation at small values of  $x$  where the spin-spin couplings are very weak is very small even deep in the ferromagnetic regime. This ‘boundary effect’ means in its ground state the system has a finite magnetic susceptibility to changes in temperature, i.e.  $\frac{dM^z}{dT}|_{T=0} = -2\ln(2)$ . In the homogeneous case we have  $\frac{dM^z}{dT}|_{T=0} = 0$ . Thus, despite the fact that both systems are mean-field in terms of their universal behaviour, they exhibit very different Physics in the ferromagnetic regime.

*Transverse Field Ising Model* – Let us move on to a second, non-classical example to highlight the depth of our results. We consider the transverse field Ising model by setting  $J^x = J^y = h^y = h^z = 0$  and  $h^x = -h, J^z = -1$  in Eq. (1). Our integral equation is then

$$\lambda^z(x) = \int_0^1 \frac{W(x,y)\lambda^z(y)\tanh\left(\beta\sqrt{h^2 + (\lambda^z(y))^2}\right)}{\sqrt{h^2 + (\lambda^z(y))^2}} dy. \quad (8)$$

We choose to exclusively focus on the ground-state by taking the limit  $\beta \rightarrow \infty$  and removing the hyperbolic tangent from the equation. In this case we can again use Banach’s fixed-point theorem to prove the existence of a disordered-ordered phase transition with an upper bound of the critical field strength  $h_c$  given by the supremum of the marginal of the graphon.

Let us treat some explicit examples. First, considering the Erdős-Rényi graphon  $W(x,y) = p$  straightforwardly yields the solution  $M^z = \sqrt{1 - \frac{h^2}{p^2}}$  consistent with a rescaled TFI model with all-to-all coupling.

There are, however, other, less trivial graphons for which an exact analytical solution for the ground state properties can still be found. For instance, consider  $W(x,y) = \sqrt{xy}$ . Some algebra on Eq. (8) (see Appendix) leads to  $\sigma^x(x) = \frac{h}{\sqrt{h^2 + g^2 x}}$  and  $\sigma^z(x) = -\frac{g\sqrt{x}}{\sqrt{h^2 + g^2 x}}$  where  $g$  is given by

$$g = \begin{cases} \frac{\sqrt{2}}{3} \sqrt{1 + (1 - 3h)\sqrt{1 + 6h}} & h < \frac{1}{2}, \\ 0 & \text{otherwise.} \end{cases} \quad (9)$$

Integrating the expression (see appendix) for the transverse magnetisation then gives the following closed form for the total transverse magnetisation density

$$M^x = \begin{cases} \frac{6h}{3h + \sqrt{2 + 9h^2 + (2 - 6h)\sqrt{1 + 6h}}} & h < \frac{1}{2}, \\ 1 & \text{otherwise.} \end{cases} \quad (10)$$

The total longitudinal magnetisation density can also be obtained in closed form (see Appendix), but it is too long to contain here in the main text. Our methodology has yielded an analytic expression for the magnetisation (in the thermodynamic limit) of the Transverse Field Ising Model on a complex, highly inhomogeneous graph structure.

In Fig. 2 we plot these analytical solutions for this graphon alongside those for the complete graph. Again, the left boundary of the system which has very weak  $z - z$  coupling modifies the physics of the system and makes it more susceptible to the transverse field than the all-to-all case. The transverse-field susceptibility versus site-index  $x$  can be derived from Eq. (9) yielding  $\lim_{h \rightarrow 0} \frac{d\langle \sigma^x(x) \rangle}{dh} | = \delta(x)$ , where  $\delta(x)$  is the Dirac-delta function. There is thus a singularity in the susceptibility on the left boundary of the system at 0 field-strength in the ferromagnetic regime. Such a singularity is not present in the all-to-all model and so distinguishes their Physics in the ferromagnetic regime. Critical exponents for the magnetisations at the phase transition can be found via expansion of the analytical results and these are consistent with the mean-field universality class and equivalent for the two graphons.

In Fig. 2 we also provide finite-size simulations of the ground state using state-of-the-art Density Matrix Renormalization Group (DMRG) [28] calculations on a Matrix Product State ansatz. The results demonstrate convergence to our analytical solution as we are able to reach system sizes on the order of  $\sim 100$  spins, well beyond exact diagonalisation. Importantly, from these numerics we can obtain the entanglement entropy of the ground state on a finite system. This is non-zero and diverges logarithmically in the vicinity of the critical point. This ‘weak’ scaling explains the success of our numerical results. It is reminiscent of the entanglement properties of 1D systems at criticality and has also been observed in other dense graph systems [29]. Such a diverging entanglement entropy whilst the ground state properties are consistent with a mean-field theory as  $L \rightarrow \infty$  is a striking result.

*Discussion and Conclusions* – We have successfully utilised tools from graph theory to derive an elegant

set of integral equations which describe the physics of generic spin models with a large density of interactions in the thermodynamic limit—whether classical or quantum. The graphon, a continuous function over the real unit square, describes the geometry of the system and forms the kernel in the corresponding equations. We have shown how our formalism reproduces well-known results and can be used to derive exact, analytical solutions for the equilibrium properties of more complex systems. Whilst the universality class of these solutions is mean-field, we observe how the inhomogeneity can dramatically alter the Physics deep inside certain regions of the phase diagram. In the main text we have focused on several examples where we can derive an explicit solution to our equations. In the Supplemental we have consider further graphons, many of which are popular within the graph theory community. We derive the reduced form of Eq. (4) for these graphons, which can be solved numerically or attacked with advanced analytical treatments.

Our work opens up a number of further avenues for future research. Firstly, extending our formalism to describe the out-of-equilibrium dynamics of a spin system on a dense graph is a natural direction. In this case the graphon would form the central object in the coupled differential equations which describe the dynamics of the  $\lambda^\alpha(x)$  functions. Whilst an analytical solution is known for the all-to-all case ( $W(x, y) = 1$ ) on the Lipkin-Meshkov-Glick model (a model whose dynamics was recently realised on a quantum simulator [30]), our graph-theoretic approach could open up solutions for a whole range of dense graphs.

Secondly, mathematical extensions to graphons for non-dense graphs have been formulated within the literature [31, 32]. Such an approach could be used to form a general continuous description of spin systems on sparse graphs—either in the mean-field limit or further.

---

[1] M. D. Shirley and S. P. Rushton, “The impacts of network topology on disease spread,” *Ecological Complexity*, vol. 2, no. 3, pp. 287–299, 2005.

[2] S. Lozano, L. Buzna, and A. Díaz-Guilera, “Role of network topology in the synchronization of power systems,” *The European Physical Journal B*, vol. 85, p. 231, Jul 2012.

[3] X. F. Wang, “Complex networks: Topology, dynamics and synchronization,” *International Journal of Bifurcation and Chaos*, vol. 12, no. 05, pp. 885–916, 2002.

[4] A. Zakharova, M. Kapeller, and E. Schöll, “Chimera death: Symmetry breaking in dynamical networks,” *Phys. Rev. Lett.*, vol. 112, p. 154101, Apr 2014.

[5] F. A. Rodrigues, T. K. D. Peron, P. Ji, and J. Kurths, “The Kuramoto model in complex networks,” *Physics Reports*, vol. 610, pp. 1–98, 2016. The Kuramoto model in complex networks.

[6] Y. Cao, V. Fatemi, S. Fang, K. Watanabe, T. Taniguchi, E. Kaxiras, and P. Jarillo-Herrero, “Unconventional superconductivity in magic-angle graphene superlattices,” *Nature*, vol. 556, pp. 43–50, Apr 2018.

[7] P. Corbae, F. Hellman, and S. M. Griffin, “Structural disorder-driven topological phase transition in noncentrosymmetric BiTeI,” *Phys. Rev. B*, vol. 103, p. 214203, Jun 2021.

[8] A. Georges, G. Kotliar, W. Krauth, and M. J. Rozenberg, “Dynamical mean-field theory of strongly correlated fermion systems and the limit of infinite dimensions,” *Rev. Mod. Phys.*, vol. 68, pp. 13–125, Jan 1996.

[9] G. Kotliar, S. Y. Savrasov, K. Haule, V. S. Oudovenko, O. Parcollet, and C. A. Marianetti, “Electronic structure calculations with dynamical mean-field theory,” *Rev. Mod. Phys.*, vol. 78, pp. 865–951, Aug 2006.

[10] A. I. Lichtenstein, M. I. Katsnelson, and G. Kotliar, “Finite-temperature magnetism of transition metals: An ab initio dynamical mean-field theory,” *Phys. Rev. Lett.*, vol. 87, p. 067205, Jul 2001.

[11] P. A. Pearce, “Mean-field bounds on the magnetization for ferromagnetic spin models,” *Journal of Statistical Physics*, vol. 25, pp. 309–320, Jun 1981.

[12] D. Yamamoto, “Correlated cluster mean-field theory for spin systems,” *Phys. Rev. B*, vol. 79, p. 144427, Apr 2009.

[13] F. L. Metz and T. Peron, “Mean-field theory of vector spin models on networks with arbitrary degree distributions,” *Journal of Physics: Complexity*, vol. 3, p. 015008, feb 2022.

[14] F. G. S. L. Brandão and A. W. Harrow, “Product-state approximations to quantum states,” *Communications in Mathematical Physics*, vol. 342, pp. 47–80, Feb 2016.

[15] L. Lovasz and B. Szegedy, “Limits of dense graph sequences,” 2004.

[16] P. J. Wolfe and S. C. Olhede, “Nonparametric graphon estimation,” 2013.

[17] M.-A. Gkogkas and C. Kuehn, “Graphon mean-field limits for Kuramoto-type models,” 2020.

[18] C. Kuehn and S. Throm, “Power network dynamics on graphons,” *SIAM Journal on Applied Mathematics*, vol. 79, no. 4, pp. 1271–1292, 2019.

[19] F. Parise and A. Ozdaglar, “Graphon games,” in *Proceedings of the 2019 ACM Conference on Economics and Computation*, EC ’19, (New York, NY, USA), p. 457–458, Association for Computing Machinery, 2019.

[20] To the best of our knowledge.

[21] A. Lipowski, D. Lipowska, and A. L. Ferreira, “Phase transition and power-law coarsening in an Ising-doped voter model,” *Phys. Rev. E*, vol. 96, p. 032145, Sep 2017.

[22] D. Stauffer, “Social applications of two-dimensional Ising models,” *American Journal of Physics*, vol. 76, no. 4, pp. 470–473, 2008.

[23] J. Majewski, H. Li, and J. Ott, “The Ising model in physics and statistical genetics,” *Am. J. Hum. Genet.*, vol. 69, pp. 853–862, Oct. 2001.

[24]  $\Lambda(x)$  is always positive here - it is the principal root.

[25] M. Nazam and M. Arshad, “On a fixed point theorem with application to integral equations,” *International Journal of Analysis*, vol. 2016, p. 9843207, May 2016.

[26] A. Bovier and V. Gayrard, “The thermodynamics of the Curie-Weiss model with random couplings,” *Journal of Statistical Physics*, vol. 72, pp. 643–664, 1993.

[27] J. Tindall, A. Searle, A. Alhajri, and D. Jaksch, “Quantum physics in connected worlds,” *Nature Communications*, vol. 13, p. 7445, Dec 2022.

[28] S. R. White, “Density matrix formulation for quantum renormalization groups,” *Phys. Rev. Lett.*, vol. 69, pp. 2863–2866, Nov 1992.

[29] J. I. Latorre, R. Orús, E. Rico, and J. Vidal, “Entanglement entropy in the Lipkin-Meshkov-Glick model,” *Phys. Rev. A*, vol. 71, p. 064101, Jun 2005.

[30] K. Xu, Z.-H. Sun, W. Liu, Y.-R. Zhang, H. Li, H. Dong, W. Ren, P. Zhang, F. Nori, D. Zheng, H. Fan, and H. Wang, “Probing dynamical phase transitions with a superconducting quantum simulator,” *Science Advances*, vol. 6, no. 25, p. eaba4935, 2020.

[31] C. Borgs, J. T. Chayes, H. Cohn, and N. Holden, “Sparse exchangeable graphs and their limits via graphon processes,” *Journal of Machine Learning Research*, vol. 18, no. 210, pp. 1–71, 2018.

[32] H. C. Christian Borgs, Jennifer T. Chayes and Y. Zhao, “An  $L^p$  theory of sparse graph convergence i: Limits, sparse random graph models, and power law distributions,” *Trans. Amer. Math. Soc.*, vol. 372, pp. 3019–3062, 2019.

[33] M. Fishman, S. R. White, and E. M. Stoudenmire, “The ITensor Software Library for Tensor Network Calculations,” *SciPost Phys. Codebases*, p. 4, 2022.

[34] E. Abbe, “Community detection and stochastic block models: Recent developments,” *Journal of Machine Learning Research*, vol. 18, no. 177, pp. 1–86, 2018.

[35] C. Borgs, J. Chayes, L. Lovász, V. Sós, and K. Vesztergombi, “Limits of randomly grown graph sequences,” *European Journal of Combinatorics*, vol. 32, no. 7, pp. 985–999, 2011. Homomorphisms and Limits.

[36] J. Hale and S. Lunel, *Introduction to Functional Differential Equations*. Applied Mathematical Sciences, Springer New York, 2013.

[37] L. Lovasz, *Large networks and graph limits*. Providence, RI: American Mathematical Society, 2012.

## I. ACKNOWLEDGEMENTS

JT is grateful for ongoing support through the Flatiron Institute, a division of the Simons Foundation. AS acknowledges funding from the UK Engineering and Physical Sciences Research Council as well as from the Smith-Westlake scholarship. We are grateful to Sam Staton, Dieter Jaksch, Dries Sels and Vadim Oganesyan for fruitful discussions. Monte-Carlo calculations were performed with code written solely by the authors whilst Density-Matrix Renormalisation Group Calculations were done with the help of the ITensor library [33].

## II. APPENDIX

### A. Mean-Field Treatment of $H(G_L)$

Here we perform a mean-field treatment of  $H(G_L)$  in Eq.(1). First, let  $\hat{\sigma}_v^\alpha = \langle \hat{\sigma}_v^\alpha \rangle + \hat{\delta}_v^\alpha$ , substitute it into the Hamiltonian and ignore terms of order  $\hat{\delta}^2$ . The result is (up to a constant):

$$H = \sum_v H_v = \sum_v \sum_\alpha \hat{\sigma}_v^\alpha \left( \frac{1}{L} \left( \sum_{v'=1}^L A_{v,v'} J^\alpha \langle \hat{\sigma}_v^\alpha \rangle \right) + h^\alpha \right). \quad (\text{S1})$$

Within this mean-field approximation the equilibrium state of the system is given by

$$\rho(\beta) = \frac{\exp(-\beta H)}{\text{Tr}(\exp(-\beta H))} = \bigotimes_{v=1}^L \frac{\exp(-\beta H_v)}{\text{Tr}(\exp(-\beta H_v))} = \bigotimes_{v=1}^L \rho_v. \quad (\text{S2})$$

Where the reduced density matrix on each site  $\rho_v$  is, explicitly (in the basis spanned by the eigenstates of  $\sigma^z$ ), the following  $2 \times 2$  matrix:

$$\rho_v = \frac{1}{2\lambda_v} \begin{pmatrix} \lambda_v - \lambda_v^z \tanh(\beta\lambda_v) & -(\lambda_v^x - i\lambda_v^y) \tanh(\beta\lambda_v) \\ -(\lambda_v^x + i\lambda_v^y) \tanh(\beta\lambda_v) & \lambda_v + \lambda_v^z \tanh(\beta\lambda_v) \end{pmatrix} \quad (\text{S3})$$

where we have defined  $\lambda_v = \sqrt{(\lambda_v^x)^2 + (\lambda_v^y)^2 + (\lambda_v^z)^2}$  and  $\lambda_v^\alpha = \frac{1}{L} \left( \sum_{v'} A_{v,v'} J^\alpha \langle \hat{\sigma}_{v'}^\alpha \rangle \right) + h^\alpha$ .

By taking the expectation values  $\langle \sigma_v^\alpha \rangle$  associated with  $\rho_v$  we find the  $\lambda_v^\alpha$  variables must obey the following self-consistency relation:

$$\lambda_v^\alpha = -\frac{1}{L} \left( \sum_{v'=1}^L \frac{J^\alpha A_{v,v'} \lambda_v^\alpha \tanh(\beta\lambda_{v'})}{\lambda_v} \right) + h^\alpha, \quad (\text{S4})$$

with  $v = 1 \dots L$  and  $\alpha = x, y, z$ . The set of values  $\{\lambda_v^\alpha\}$  with  $v = 1 \dots L$ ,  $\alpha = x, y, z$  which solves the  $3L$  non-linear equations described by Eq. (5) thus fully characterise the mean-field equilibrium state associated with  $H$ .

Now we wish to take the continuum limit of Eq. (S4). First, we define the following:  $x = v/L$ ,  $dx = 1/L$ ,  $\lambda_v^\alpha = \lambda^\alpha(x)$  and  $\lambda_v = \lambda(x)$ . Now let us assume that the adjacency matrix has been generated as a discrete realisation of some graphon  $W(x, y)$ , i.e.  $A_{v,v'} = L^2 \int_{I_v \times I_{v'}} W(x, y) dx dy$ ,  $I_v = [(v-1)/L, v/L]$ . Substituting this all into Eq. (S4) gives us

$$\lambda^\alpha(x) = - \left( \sum_{y=1/L, 2/L, \dots, L} \frac{J^\alpha L^2 \left( \int_{I_v \times I_{v'}} W(x, y) dx dy \right) \lambda^\alpha(y) \tanh(\beta\lambda(y))}{\lambda(y)} \right) dx + h^\alpha. \quad (\text{S5})$$

Now we take  $L \rightarrow \infty$  which implies  $L^2 \left( \int_{I_v \times I_{v'}} W(x, y) dx dy \right) \rightarrow W(x, y)$  and the summation becomes an integral. We can then write down the coupled, continuous mean-field equations

$$\lambda^\alpha(x) = -J^\alpha \int_0^1 \frac{W(x, y) \lambda^\alpha(y) \tanh(\beta\Lambda(y))}{\Lambda(y)} dy + h^\alpha, \quad (\text{S6})$$

with  $\alpha = x, y, z$  and  $\Lambda(x) = \sqrt{(\lambda^x(x))^2 + (\lambda^y(x))^2 + (\lambda^z(x))^2}$ . These govern our system in the thermodynamic limit of the sequence of graphs generated from the graphon  $W(x, y)$ . They are coupled, non-linear Fredholm integral equations with the graphon acting as the Kernel. From the solution set  $\{\lambda^x(x), \lambda^y(x), \lambda^z(x)\}$  to these equations we can obtain the on-site magnetisations via

$$\sigma^\alpha(x) = -\frac{\lambda^\alpha(x) \tanh(\beta\Lambda(x))}{\Lambda(x)} \quad (\text{S7})$$

and the total magnetisation density is  $M^\alpha = \int_0^1 \sigma^\alpha(x) dx$ .

## B. Proof of Theorem 1.

We restate the Hamiltonian from the main text

$$H(G_L) = \frac{1}{L} \sum_{\substack{v, v' = 1 \\ v > v'}}^L A_{v, v'} \left( \sum_{\alpha=x, y, z} J^\alpha \hat{\sigma}_v^\alpha \hat{\sigma}_{v'}^\alpha \right) + \sum_{\substack{v \in V \\ \alpha=x, y, z}} h^\alpha \hat{\sigma}_v^\alpha, \quad (\text{S8})$$

where all terms remain as defined in the main text. We now prove Theorem 1 from the main text, which is restated below.

**Theorem 1** *Let  $f(A) = -\frac{1}{L\beta} \ln(\text{Tr}(\exp(-\beta A)))$  be the free energy density of a  $d^L \times d^L$  matrix, with  $\beta \in \mathbb{R}_{\geq 0}$ . Let  $G_L^R$  be the random-exchange realisation on  $L$  vertices of a graphon  $W(x, y)$ . Let  $G_L^D$  be a weighted graph on  $L$  vertices whose adjacency matrix  $A^D$  is specified by the elements  $A_{v, v'}^D = P_{v, v'}$ , with  $P_{v, v'}$  defined from  $W(x, y)$  as in Eq. (2). Then for an arbitrary set of real, finite values for the parameters  $\{J^x, J^y, J^z, h^x, h^y, h^z\}$  the following is true*

$$|f(H(G_L^R)) - f(H(G_L^D))| = \mathcal{O}(L^{-1/2}), \quad (\text{S9})$$

which vanishes in the limit  $L \rightarrow \infty$ .

We recall a Lemma proven in [27], which we will be helpful in completing the proof.

**Lemma 1** *Let  $(A_n)_{n \in \mathbb{Z}} = (A_1, A_2, \dots)$  and  $(B_n)_{n \in \mathbb{Z}} = (B_1, B_2, \dots)$  be two sequences of Hermitian matrices. The matrices  $A_L$  and  $B_L$  in the sequence have size  $d^L \times d^L$ , with  $d$  fixed. Let  $D_L = A_L - B_L$  and  $\lambda_{\max}^D$  be the largest (in terms of the absolute value) eigenvalue of  $D_L$ . If  $|\lambda_{\max}^D| = \mathcal{O}(L^\kappa)$  then  $|f(A_L) - f(B_L)| = \mathcal{O}(L^{\kappa-1})$ , which vanishes for  $\kappa < 1$  as  $L \rightarrow \infty$ .*

We begin by defining the following operator:

$$D_L = H(G_L^R) - H(G_L^D) = \sum_{\alpha=x, y, z} D_L^\alpha = \sum_{\alpha=x, y, z} \frac{1}{L} \left( \sum_{\substack{i, j=1 \\ i < j}}^L A_{ij} \hat{\sigma}_i^\alpha \hat{\sigma}_j^\alpha - \sum_{\substack{i, j=1 \\ i < j}}^L A_{ij}^D \hat{\sigma}_i^\alpha \hat{\sigma}_j^\alpha \right), \quad (\text{S10})$$

where  $A_{ij}$  are the matrix elements of the random exchange graph  $G_L^R$ .

We proceed to evaluate the eigenvalues of the operator  $D_L^\alpha$ . As such, consider its eigenstates  $|\sigma_1^\alpha, \dots, \sigma_L^\alpha\rangle$ , where  $\hat{\sigma}_i^\alpha |\sigma_1^\alpha, \dots, \sigma_L^\alpha\rangle = \mu_i |\sigma_1^\alpha, \dots, \sigma_L^\alpha\rangle$ , with  $\mu_i = \pm 1$ , depending on whether the  $i$ th spin is pointing ‘up’ or ‘down’ in that basis. We will define  $\mu_{ij} := \mu_i \mu_j$  and consider the eigenvalue

$$\langle \sigma_1^\alpha, \dots, \sigma_L^\alpha | D_L^\alpha | \sigma_1^\alpha, \dots, \sigma_L^\alpha \rangle = \frac{1}{L} \left( \sum_{\substack{i, j=1 \\ i < j}}^L A_{ij} \mu_{ij} - \sum_{\substack{i, j=1 \\ i < j}}^L A_{ij}^D \mu_{ij} \right), \quad (\text{S11})$$

We will proceed to show that, independent of the eigenstate  $|\sigma_1^\alpha, \dots, \sigma_L^\alpha\rangle$ , this eigenvalue grows, at most, as  $L^{1/2}$  in the large  $L$  limit. From there we can invoke Weyl’s inequality to show that the eigenvalues of  $D_L$  grow asymptotically as  $L^{1/2}$  and subsequently invoke Lemma 1 (from above) to complete the proof of Theorem 1.

To prove the  $L^{1/2}$  growth of Eq. (S11), we begin with the Hoeffding inequality. This states that for independent random variables  $Y_1, \dots, Y_n$  for which  $a_i \leq Y_i \leq b_i$  then the sum  $S_n := Y_1 + Y_2 + \dots + Y_n$  is bounded as

$$P(|S_n - \mathbb{E}(S_n)| \geq t) \leq 2 \exp \left( - \frac{2t^2}{\sum_{i=1}^n (a_i - b_i)^2} \right), \quad (\text{S12})$$

with the factor of 2 stemming from the fact we have incorporated both the upper and lower Hoeffding bounds together. We will apply this bound to Eq. (S11).

Let us construct the set  $X := \{X_{ij}\}$  which consists of the  $\frac{L(L-1)}{2}$  random variables  $X_{ij} := A_{ij} \mu_{ij}$  (we have  $i, j = 1 \dots L$  and  $i > j$ ). Observe that since  $A_{ij} \in \{0, 1\}$  and  $\mu_{ij}$  is either 1 or  $-1$ , we have that  $-1 \leq X_{ij} \leq 1$ . Also,  $\mathbb{E}(X_{ij}) = \mathbb{E}(A_{ij}) \mu_{ij} = A_{ij}^D \mu_{ij}$ , where  $\mathbb{E}(A_{ij})$  denotes the expected value. In our case, however, all of the  $X_{ij}$  quantities are not independent—the sign of  $X_{ij}$  is determined from the sign of  $X_{ik}$  and  $X_{kj}$ . This can be dealt with by applying the Hoeffding bound to the  $X_{ij}$ ’s with positive and negative sign separately.

A given eigenvector  $|\sigma_1^\alpha, \dots, \sigma_L^\alpha\rangle$  will consist of a number of spins pointing up ( $\sigma_i = +1$ ) and the remainder pointing down ( $\sigma_i = -1$ ). Define  $M = \sum_{k=1}^L \sigma_k$ , then it can be checked that of the  $\frac{L(L-1)}{2}$  parameters  $\mu_{ij}$ ,  $\frac{L^2+M^2-2L}{4}$  are positive and  $\frac{L^2-M^2}{4}$  are negative. We therefore partition the set  $X := \{X_{ij}\}$  into two sets as follows

$$\begin{cases} x^A := \{X_{ij} | \mu_{ij} = 1\}, \\ x^B := \{X_{ij} | \mu_{ij} = -1\} \end{cases}$$

We would like also to keep track of the values  $A_{ij}^D \mu_{ij}$ , so we partition the set  $\{\mu_{ij} A_{ij}^D\}$  into

$$\begin{cases} \bar{x}^A := \{\mu_{ij} A_{ij}^D | \mu_{ij} = 1\}, \\ \bar{x}^B := \{\mu_{ij} A_{ij}^D | \mu_{ij} = -1\} \end{cases}$$

We can now invoke the Hoeffding bound on each set separately, since each set now consists on independent random variables. We have two sums on which to invoke the bound:  $S^A := \sum_{l=1}^{\frac{M^2+L^2-2L}{4}} x_l^A$  and  $S^B := \sum_{l=1}^{\frac{L^2-M^2}{4}} x_l^B$ , where we use  $x_l^A$  and  $x_l^B$  to refer to elements from  $x^A$  and  $x^B$  respectively. Likewise we will use  $\bar{x}_i^A$  and  $\bar{x}_i^B$  to refer to individual elements of  $\bar{x}^A$  and  $\bar{x}^B$  respectively. Then observe that, due to  $\mathbb{E}(X_{ij}) = A_{ij}^D \mu_{ij}$  we have  $\mathbb{E}(S^A) = \sum_{l=1}^{\frac{M^2+L^2-2L}{4}} \bar{x}_l^A$  and  $\mathbb{E}(S^B) = \sum_{l=1}^{\frac{L^2-M^2}{4}} \bar{x}_l^B$

Equation (S12) then gives two bounds:

$$\begin{cases} P(|S^A - \mathbb{E}(S^A)| \geq t_1) \leq 2 \exp\left(\frac{-2t_1^2}{L^2+M^2-2L}\right), \\ P(|S^B - \mathbb{E}(S^B)| \geq t_2) \leq 2 \exp\left(\frac{-2t_2^2}{L^2-M^2}\right). \end{cases}$$

We combine these bounds to obtain:

$$P\left(\left|\sum_{\substack{i,j=1 \\ i < j}}^L \mu_{ij} A_{ij} - \sum_{\substack{i,j=1 \\ i < j}}^L \mu_{ij} A_{ij}^D\right| \geq t_1 + t_2\right) \leq 4 \exp\left(\frac{-2t_1^2}{L^2+M^2-2L}\right) \exp\left(\frac{-2t_2^2}{L^2-M^2}\right). \quad (\text{S13})$$

Since we fixed the magnetisation  $M$  of the eigenstate in deriving the above bound, we should take the union bound over  $\binom{L}{\frac{1}{2}(L+M)}$  eigenstates with magnetisation  $M$ . We will denote an eigenstate with magnetisation  $M$  as  $|\sigma_M\rangle$ , resulting in the new bound

$$\bigcup_{|\sigma_M\rangle} P\left(\left|\sum_{\substack{i,j=1 \\ i < j}}^L \mu_{ij} A_{ij} - \sum_{\substack{i,j=1 \\ i < j}}^L \mu_{ij} A_{ij}^D\right| \geq t_1 + t_2\right) \leq 4 \binom{L}{\frac{1}{2}(L+M)} \exp\left(\frac{-2t_1^2}{L^2+M^2-2L}\right) \exp\left(\frac{-2t_2^2}{L^2-M^2}\right). \quad (\text{S14})$$

Now observe that the following is true

$$\binom{L}{\frac{1}{2}(L+M)} \exp\left(\frac{-2t_1^2}{L^2+M^2-2L}\right) \exp\left(\frac{-2t_2^2}{L^2-M^2}\right) \leq \binom{L}{\frac{L}{2}} \exp\left(-\frac{t_1^2+t_2^2}{L^2}\right), \quad (\text{S15})$$

where  $L \in \mathbb{N}$ ,  $|M| \leq L$  and  $t_1, t_2 \in \mathbb{R}^+$ . This leads us to the following

$$\bigcup_M \bigcup_{|\sigma_M\rangle} P\left(\left|\sum_{\substack{i,j=1 \\ i < j}}^L \mu_{ij} A_{ij} - \sum_{\substack{i,j=1 \\ i < j}}^L \mu_{ij} A_{ij}^D\right| \geq t_1 + t_2\right) \leq 4(L+1) \binom{L}{\frac{L}{2}} \exp\left(-\frac{t_1^2+t_2^2}{L^2}\right), \quad (\text{S16})$$

where the union bound has again been used. Now observe that if  $t_1 + t_2 = \mathcal{O}(L^\gamma)$  then  $t_1^2 + t_2^2 = \mathcal{O}(L^{2\gamma})$ , where  $\gamma \in \mathbb{R}$ . Using the fact  $\binom{L}{\frac{L}{2}} \sim \sqrt{\frac{2}{L\pi}} 2^L$  for large  $L$ , and also that using  $2^L = e^{L\ln(2)}$ , we then arrive at

$$\bigcup_M \bigcup_{|\sigma_M\rangle} P\left(\left|\sum_{\substack{i,j=1 \\ i < j}}^L \mu_{ij} A_{ij} - \sum_{\substack{i,j=1 \\ i < j}}^L \mu_{ij} A_{ij}^D\right| \geq \mathcal{O}(L^\gamma)\right) \leq 2(L+1) \sqrt{\frac{2}{L\pi}} \exp(L\ln(2) - \mathcal{O}(L^{2\gamma-2})), \quad (\text{S17})$$

which vanishes unless  $\gamma \leq \frac{3}{2}$ . This leads us to

$$\langle \sigma_1^\alpha, \dots, \sigma_L^\alpha | D_L^\alpha | \sigma_1^\alpha, \dots, \sigma_L^\alpha \rangle = \mathcal{O}(L^{\frac{1}{2}}) \quad \forall M, |\sigma|. \quad (\text{S18})$$

Now from Weyl's inequality we know that the eigenvalues of the operator  $D_L = H(G_L^R) - H(G_L^D)$  are therefore bounded as  $\mathcal{O}(L^{1/2})$ . From here we can invoke Lemma 1 with  $\kappa = 1/2$  and Theorem 1 is proven.

### C. Analytical Solution of the Classical Ising Model for $W(x, y) = xy$

We wish to solve Eq. (6) with  $W(x, y) = xy$ , i.e. identify the function  $\lambda^z(x)$  which solves

$$\lambda^z(x) = \int_0^1 xy \tanh(\beta \lambda^z(y)) dy. \quad (\text{S19})$$

We start by observing that  $\lambda^z(x) = f(\beta)x$ , where  $f(\beta)$  is a real valued function of  $\beta$  that is independent of  $x$ . Substituting this into Eq. (S19) and defining  $c = \beta f(\beta)$  gives us

$$\frac{c}{\beta} = \int_0^1 y \tanh(cy) dy, \quad (\text{S20})$$

We can perform the integration here analytically. First, perform integration by parts and expand into exponentials:

$$\int_0^1 y \tanh(cy) dy = \frac{1}{c^2} \left( \left[ \frac{1}{2} y^2 \tanh(cy) \right]_0^c - \frac{1}{2} \int_0^c y^2 \operatorname{sech}^2(y) dy \right) = \frac{1}{c^2} \left( \frac{c^2 \tanh(c^2)}{2} - \int_0^c \frac{2y^2 e^{-2y}}{(1 + e^{-2y})^2} dy \right). \quad (\text{S21})$$

Now the integral on the RHS can be dealt with by observing that  $\frac{e^{-2y}}{(1 + e^{-2y})^2} = \sum_{n=1}^{\infty} (-1)^{n-1} n e^{-2ny}$ , giving us

$$c^2 \int_0^1 y \tanh(cy) dy = \frac{c^2 \tanh(c^2)}{2} - \sum_{n=1}^{\infty} (-1)^{n-1} n \int_0^c 2y^2 e^{-2ny} dy = \frac{c^2 \tanh(c^2)}{2} - \sum_{n=1}^{\infty} \frac{(-1)^n (1 + e^{-2cn}) (1 + 2cn(1 + cn))}{2n^2}. \quad (\text{S22})$$

We can evaluate the series by splitting up the numerator and using known results,

$$c^2 \int_0^1 y \tanh(cy) dy = \frac{1}{2} - \frac{\pi^2}{24c^2} + \frac{1}{c} \ln(1 + e^{-2c}) - \frac{1}{2c^2} \operatorname{PL}_2(-e^{-2c}). \quad (\text{S23})$$

We can then use this result to reduce Eq. (S19) to Eq. (7) from the main text:

$$\frac{1}{\beta} = \frac{1}{24c^3} (12c^2 - \pi^2 + 24 \operatorname{cln}(1 + e^{-2c}) - 12 \operatorname{PL}_2(-e^{-2c})). \quad (\text{S24})$$

Additionally, it is straightforward to observe that  $M^z = \int_0^1 \sigma^z(x) dx = \int_0^1 \tanh(cx) dx = \frac{\ln(\cosh(c))}{c}$ .

### D. Analytical Solution of the Ground-State of the Transverse Field Ising Model for $W(x, y) = \sqrt{xy}$

We wish to solve Eq. (8) with  $W(x, y) = \sqrt{xy}$  and  $\beta = \infty$ , i.e:

$$\lambda^z(x) = \sqrt{x} \int_0^1 \frac{\sqrt{y} \lambda^z(y)}{\sqrt{h^2 + (\lambda^z(y))^2}} dy, \quad (\text{S25})$$

again observing that this implies  $\lambda^z(x) = \sqrt{x} g(h)$  where  $g(h)$  is some real-valued function of  $h$  gives

$$\int_0^1 \frac{y}{\sqrt{h^2 + g^2(h)y}} dy = 1, \quad (\text{S26})$$

which we can solve for  $g(h)$  (we restrict  $h$  and  $g(h)$  to be positive real without loss of generality) by a series of substitutions. Yielding

$$\frac{2(2h^3 - 2h^2\sqrt{h^2 + g^2(h)} + g^2(h)\sqrt{h^2 + g^2(h)})}{3g^4(h)} = 1, \quad (\text{S27})$$

which has the solution

$$g(h) = \begin{cases} \frac{\sqrt{2}}{3}\sqrt{1 + (1 - 3h)\sqrt{1 + 6h}} & h < \frac{1}{2}, \\ 0 & \text{otherwise.} \end{cases} \quad (\text{S28})$$

as in the main text. The transverse and longitudinal magnetisations are determined by the integrals  $M^x = \int_0^1 \frac{h}{\sqrt{h^2 + g^2(h)x}} dx$  and  $M^z = -\int_0^1 \frac{g(h)\sqrt{x}}{\sqrt{h^2 + g^2(h)x}} dx$  respectively. The first, by direct integration, yields Eq. (10) as in the main text. The second can be done by an extensive series of trigonometric substitutions and results in the following closed form expression

$$M^z(x) = \begin{cases} \frac{(1+s)\left(2\sqrt{(1-s)(4+18h^2-4s)}-9h^2(2\ln(3)+2\ln(h)-2\ln(-\sqrt{2-2s}+\sqrt{2+9h^2-2s}))\right)}{108h^2(-1+2h)} & \\ 0 & \text{otherwise} \end{cases}, \quad (\text{S29})$$

where  $s = (-1 + 3h)\sqrt{1 + 6h}$ .

### E. Further Example Graphons

In this section we consider further graphons which weren't treated in the main text but frequently appear in the literature on graphons.

*Stochastic Block Models* - The Stochastic Block Graphon is typically utilised in statistical analysis of networks because they are useful in uncovering clustering in networks [34].

The graphon can be expressed as

$$W(x, y) := \begin{cases} p_{11} & \text{if } (x, y) \in X_1 \times X_1, \\ p_{12} & \text{if } (x, y) \in X_1 \times X_2, \\ \dots & \\ p_{kk} & \text{if } (x, y) \in X_k \times X_k, \end{cases} \quad (\text{S30})$$

with  $p_{ij} = p_{ji}$  and the  $X_i$  specifying disjoint sub-domains of  $[0, 1]$  such that  $\cup_{i=1}^k X_i = [0, 1]$ . We write  $\Delta X_i$  to indicate the width of the interval  $X_i$ . The continuous mean-field equations then take on the following form

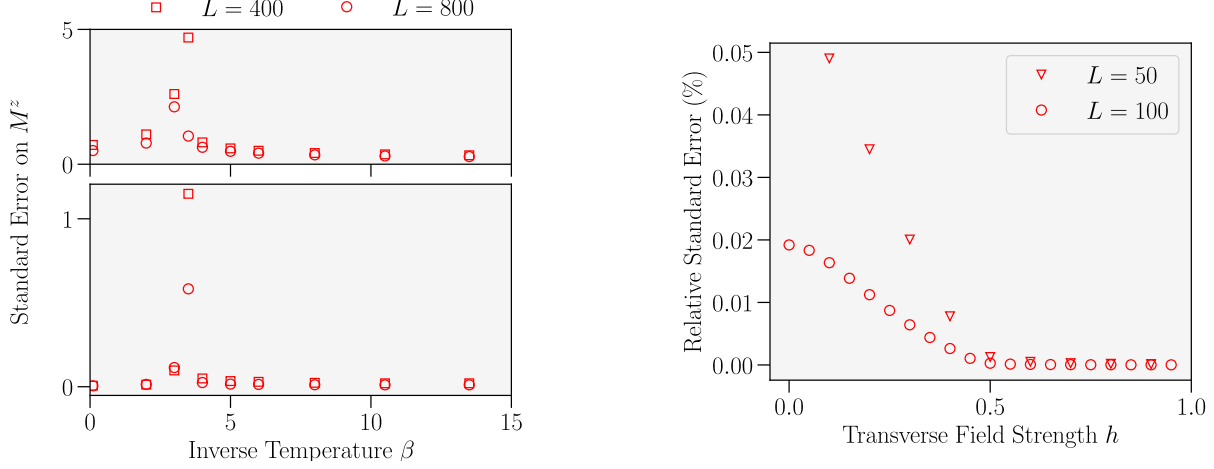
$$\lambda^\alpha(x) = -J^\alpha \sum_{j=1}^k \int_{X_j} \frac{p_{ij} \lambda^\alpha(y) \tanh\left(\beta \sqrt{(\lambda^x(y))^2 + (\lambda^y(y))^2 + (\lambda^z(y))^2}\right)}{\sqrt{(\lambda^x(y))^2 + (\lambda^y(y))^2 + (\lambda^z(y))^2}} dy + h^\alpha \quad \forall x \in X_i. \quad (\text{S31})$$

Observe that we can immediately infer from this that  $\lambda^\alpha(x)$  is constant across each of the domains  $X_i$ . We can thus define  $\lambda_i^\alpha = \lambda^\alpha(x)$   $\forall x \in X_i$  and reduce Eq. (S32) to

$$\lambda_i^\alpha = -J^\alpha \sum_{j=1}^k \Delta X_j \frac{p_{ij} \lambda_j^\alpha \tanh\left(\beta \sqrt{(\lambda_j^x)^2 + (\lambda_j^y)^2 + (\lambda_j^z)^2}\right)}{\sqrt{(\lambda_j^x)^2 + (\lambda_j^y)^2 + (\lambda_j^z)^2}} + h^\alpha, \quad (\text{S32})$$

a series of equations which become increasingly complicated to solve as the number of clusters does. In the case of a single cluster we recover the case of an Erdős-Rényi graph.

*Growing Uniform Attachment* - The growing uniform attachment graphon is given by  $W(x, y) = 1 - \max(x, y)$  [35]. The graphs which are finite realisations of this graphon will consist of nodes in which the average connectivity of a node varies uniformly across the graph. Such graphs are therefore highly inhomogenous in their average vertex



Supplementary Figure 1. a) Standard Error on the Mean for the Monte-Carlo calculations of  $M^z$  for the Classical Ising Model on finite-size realisations of  $W(x, y) = xy$ . Top plot is standard error on the mean from 5000 Monte-Carlo samples of  $M^z$  at a given  $\beta$  and  $L$ . Data points are averaged over 100 random-exchange realisations of  $W(x, y)$ . Bottom plot is the standard error on the mean from the 100 random-exchange realisations of  $W(x, y)$ , averaged over the 5000 samples taken for each realisation. b) Relative Standard Error on the Mean (Standard Error on the mean as a percentage of the mean) for the ground state energy of the Transverse Field Ising calculated via DMRG. Standard Error is that originating from the 50 random exchange realisations of  $W(x, y) = \sqrt{xy}$  at a given  $h$  and system size  $L$ .

connectivity. Substituting  $W(x, y) = 1 - \max(x, y)$  into Eq. (S6) and differentiating the left and right hand sides twice with respect to  $x$  leads us to the following coupled second-order ODEs

$$\frac{d^2\lambda^\alpha(x)}{dx^2} = J^\alpha \frac{\lambda^\alpha(x) \tanh(\beta \sqrt{\lambda^x(x)^2 + \lambda^y(x)^2 + \lambda^z(x)^2})}{\sqrt{\lambda^x(x)^2 + \lambda^y(x)^2 + \lambda^z(x)^2}}, \quad \alpha = x, y, z, \quad (\text{S33})$$

with boundary conditions  $\lambda^\alpha(1) = 0$  and  $\frac{d\lambda^\alpha(x)}{dx}|_{x=0} = 0 \forall \alpha$ .

*Maximally Irregular Graph* — The maximally irregular graph is the finite connected graph where each site (other than one pair) has a different co-ordination number to any others [27]. Taking the thermodynamic limit of the adjacency matrix results in the graphon

$$W(x, y) = \begin{cases} 1 & x + y \leq 1 \\ 0 & \text{otherwise.} \end{cases} \quad (\text{S34})$$

and the integral equations in Eq. (S32) reduce (upon differentiation) to the following three coupled first order ODEs

$$\frac{d\lambda^\alpha(x)}{dx} = -J^\alpha \frac{\lambda^\alpha(1-x) \tanh(\beta \sqrt{(\lambda_j^x(1-x))^2 + (\lambda_j^y(1-x))^2 + (\lambda_j^z(1-x))^2})}{\sqrt{(\lambda_j^x(1-x))^2 + (\lambda_j^y(1-x))^2 + (\lambda_j^z(1-x))^2}}, \quad \alpha = x, y, z, \quad (\text{S35})$$

with boundary conditions  $\lambda^\alpha(1) = 0 \forall \alpha$ . Such equations are known as functional differential equations and have been studied extensively in both Mathematics and the applied Sciences [36].

## F. Numerical Details

We provide further details about the numerical calculations which support our analytical results.

*Classical Ising Model* — For the finite-size data plotted in Figure 1 of the main text we used Monte-Carlo simulations. Specifically, for a given  $L$  we drew a finite random-exchange realisation of the graphon  $W(x, y) = xy$  and for a given

temperature  $\beta$  utilised the Metropolis-Hastings algorithm to generate  $N_{\text{Samples}} = 5000$  for the Magnetisation Density  $M^z$ . We used a Markov chain length of 250 between each sample and threw away the first 1000 samples. For each  $L$  we took 100 random-exchange realisations of the graphon  $W(x, y)$  and averaged our results over this. There are thus two sources of statistical error in our simulations: the error from sampling a finite number of random exchange realisations and the error from taking a finite number of Monte-Carlo samples. In Fig. 1 we plot the standard error on the mean from both of these sources, the values are negligible in comparison to the scale (0 → 1) of Fig. 1 in the main text.

*Transverse Ising Model* — For the data plotted in Figure 2 of the main text we used the Density-Matrix-Renormalisation-Group (DMRG) algorithm to find the ground-state of the Transverse Field Ising model. For a given  $L$  we drew a finite random-exchange realisation of the graphon  $W(x, y) = \sqrt{xy}$ . Then, for a given field strength  $h$  we took a random Matrix Product State with a small bond dimension  $\chi$  and successively performed DMRG sweeps, letting the bond-dimension double every 4th sweep until the energy converges to within 0.1% of that for the previous bond dimension. There is thus only one source of statistical error in this simulation: the error from sampling a finite number (50) of random exchange realisations. In Fig. 1 we plot this error as a percentage and observe that it is negligible (on the order of 0.01). We emphasize that the ordering of the sites (from left to right) of the Matrix Product State was taken to be identical to the ordering  $v = 1 \dots L$  of the sites of the graph.

#### G. The Graphon as the Limit Object of Dense Graph Sequences

We provide mathematical details on how the graphon  $W$  is the limit object of a sequence of dense graphs  $(G_n)_{n \in \mathbb{N}}$  where  $n$  is the number of vertices. This Appendix closely follows Ref. [37], although the theory on graph limits was first developed in [15]. The interested reader should consult either of these for more detail.

Consider two simple graphs  $F$  and  $G$ , where we define the number of vertices of  $F$  to be  $k$  and that of  $G$  to be  $n$ . A homomorphism from  $F$  to  $G$  is a map which preserves edges. This means that given an edge  $(i, j) \in E(F)$  in the set of edges  $E(F)$ , and a homomorphism  $h$ , there is always an edge  $(h(i), h(j)) \in E(G)$ —the set of edges of  $G$ . Let  $\text{hom}(F, G)$  indicate the number of homomorphisms from  $F$  into  $G$ . The homomorphism density  $t(F, G)$  is then defined to be

$$t(F, G) = \frac{\text{hom}(F, G)}{n^k}. \quad (\text{S36})$$

The homomorphism density is the probability of a random map from the graph  $F$  to the graph  $G$  being a homomorphism, since  $n^k$  is the total number of maps from a graph with  $n$  vertices to a graph with  $k$  vertices.

Suppose that instead we are given a graphon, such as  $W_G$ —the stepped graphon corresponding to the graph  $G$  which is defined as  $W_G(x, y) = A_{v, v'}$  for  $(x, y) \in [(v - 1)/n, v/n] \times [(v' - 1)/n, v'/n]$  (with  $A$  being the adjacency matrix of  $G$ ). In this case, the homomorphism density is defined to be

$$t(F, W_G) = \int_{[0,1]^k} \prod_{(i,j) \in E(F)} W(x_i, x_j) \prod_{i \in 1:k} dx_i \quad (\text{S37})$$

Here the same definition holds for any arbitrary graphon  $W$ .

The homomorphism density with reference to a finite graph  $F$  indicates the relative likelihood of the graph  $G$  or more generally graphon  $W$  containing an instance of  $F$  inside of it. If two graphs or graphons have similar homomorphism densities for *all* simple graphs  $F$ , then these graphs are similar. The definition of convergence of a sequence of graphs hinges precisely on this concept.

**Definition 1 (Convergent Graph Sequence)** *A sequence  $(G_n)$  of simple graphs with  $V(G_n) \rightarrow \infty$  as  $n \rightarrow \infty$  converges if the subgraph densities  $t(F, G_n)$  converge for all simple graphs  $F$ .*

The above definition gives allows us to precisely define in what sense  $W$  can be considered a limit object.

**Theorem 2 (Lovasz, 2012 [37])** *Let  $(G_n)$  be a sequence of simple graphs with  $V(G_n) \rightarrow \infty$ . If  $(G_n)$  converges, there exists a graphon  $W$  such that  $t(F, G_n) \rightarrow t(F, W)$  for all simple graphs  $F$ .*

The above theorem tells us that if the sequence  $(G_n)$  converges, then there exists some limit object—the graphon—which captures the limiting homomorphism density counts of the sequence of graphs for *all* simple graphs.

There is a second, equivalent, definition of convergence which us allows us to define  $W$  as an appropriate limit of a sequence of dense graphs. This definition utilises the cut distance of two graphs.

**Definition 2 (Cut Distance)** Given two graphons  $W$  and  $W'$ , define the cut distance between them to be

$$\delta_{\square}(W, W') := \inf_{\phi, \psi} \sup_{S, T} \left| \int_{S \times T} (W(\phi(x), \phi(y)) - W'(\psi(x), \psi(y))) \right| \quad (\text{S38})$$

where the infimum is taken over all vertex re-labelings  $\phi$  of  $W$  and  $\psi$  of  $W'$ . The supremum is taken over all measurable subsets  $S$  and  $T$  of  $[0, 1]$ .

The cut distance is a metric on the space of graphons (up to weak isomorphism). It maximises the difference between the integral of the two graphons on measurable intervals  $S$  and  $T$  which together form a box  $S \times T$ . This step can be thought of as maximising the difference in edges between those vertices contained in  $S \times T$ . The infimum is then taken on that chosen interval over all measure preserving maps, in order to ensure that the cut distance is zero for weakly isomorphic graphons. The following theorem can then be proven from the above definitions.

**Theorem 3 (Lovasz, 2012 [37])** Given a sequence  $(G_n)$  of simple graphs with  $|V(G_n)| \rightarrow \infty$  as  $n \rightarrow \infty$ , the sequence is said to converge to the graphon  $W$  if  $\delta_{\square}(W_{G_n}, W) \rightarrow 0$  as  $n \rightarrow \infty$ .

This theorem provides alternative definition for the graphon as a limit object. In this definition, we envisage instead the pixelated adjacency matrix of the sequence of simple graphs  $G_n$  approaching (via the cut distance) that of the limit object  $W$ .

Importantly, the above definitions and theorems can be generalised to sequences of weighted graphs by requiring the graphs to have uniformly bounded edgeweights. Moreover, we emphasise that these limits only make sense for sequences of *dense* graphs, because it can be shown that sparse graph sequences always have as their limit the graphon  $W(x, y) = 0$  for all  $x$  and  $y$ .